Journal of Applied Polymer Science

Effect of unfunctionalized and HNO_3-functionalized MWCNT on the mechanical and electrical performances of PEMFC bipolar plates

Nafaa Athmouni,[1,2] Frej Mighri,[1,2] Saïd Elkoun[1,3]
[1]Research Center for High Performance Polymer and Composite Systems, CREPEC
[2]Department of Chemical Engineering, Laval University, QC G1A 0A6, Canada
[3]Department of Mechanical Engineering, Université de Sherbrooke, QC J1K 2R1, Canada
Correspondence to: F. Mighri (E-mail: Frej.Mighri@gch.ulaval.ca)

ABSTRACT: This study aims at developing lightweight and high performance electrically conductive nanocomposites for proton exchange membrane fuel cell (PEMFC) bipolar plates (BPPs). These composites were made from an optimized co-continuous mixture of Polyethylene terephthalate (PET) and polyvinylidene fluoride (PVDF) reinforced with highly conductive carbon additives composed of carbon black (CB) and synthetic graphite (GR). Multiwall carbon nanotubes (MWCNT) were functionalized then used to improve BPPs electrical conductivity and their mechanical properties, such as flexural and impact strengths. It was observed that the best BPP prototype was obtained using nitric acid (HNO_3)-functionalized MWCNT. The latter led to the smothest BPP surface, the lowest through-plane resitivity (0.12 Ω cm) and the highest impact and flexural strengths. These results are attributed to the improved dispersion of the functionalized MWCNT, a result of their best compatibilization with the (PET/PVDF) polymeric phase. © 2016 Wiley Periodicals, Inc. J. Appl. Polym. Sci. **2016**, *133*, 43624.

KEYWORDS: batteries and fuel cells; composites; conducting polymers; mechanical properties; nanostructured polymers

Received 13 October 2015; accepted 13 March 2016
DOI: 10.1002/app.43624

INTRODUCTION

PEMFCs operating at low temperature and high power density have been regarded as attractive and environmental friendly power sources for stationary, mobile and portable applications. In addition, they help to significantly reduce pollutant emissions. The most heavy and costly components in PEMFC stacks are the BPPs, which account for about 60% of total weight and around 45% of stack cost.[1] The investigation on low cost and performant materials for BPPs is then a critical issue and a verity of conductive materials have been proposed, such as machined graphite, coated metals, and conductive polymer composites.[2–5]

Polymer composites based on thermoplastic matrices are advantageous compared to other materials with regards to their high corrosion resistance,[2] low machining cost, and low weight.[6] We already developed, by twin-screw extrusion process, BPP materials based on a co-continuous binary polymer system of PET and PVDF in which CB and synthetic GR conductive additives were incorporated.[7,8] These conductive materials allowed us to develop a BPP prototype having a through-plane resistivity of around 0.3 Ω·cm. We also showed that the conductive CB/GR additives were largely localized in the PET phase and formed a good conductive network in that phase, which largely reduced the BPP through-plane resistivity.

Generally, the objective of the research on PEMFC BPPs is to target the requirements presented by the fuel cell technologies program of the U.S. Department of Energy (USDOE).[9] To achieve the USDOE electrical conductivity requirement, conductive fillers, such as CB, have to be dispersed inside the polymeric matrix. However, high concentrations of solid CB additive provoke a significant decrease in both strength and ductility and a also a drastic increase of blend viscosity. Mighri *et al.*[10] showed that the maximum CB concentration that can be incorporated into a PET/PVDF matrix using a 17 mm Thermo-Hake corotating twin-screw extruder was around 20 wt %. Higher CB concentrations led to extrusion difficulties, such as die blockage and extruded sheet brittleness. To avoid these difficulties, synthetic GR, which is known for its good lubricating properties and high electrical conductivity, was added to the blend to increase its conductivity without any considerable changes in blend processability.[8] However, high amounts of GR are needed to attain the DOE electrical conductivity target value, leading to extremely brittle BPs. To overcome this issue, carbon nanotubes (CNT) can be added in a small quantity to improve BP electrical conductivity without a drastic change in

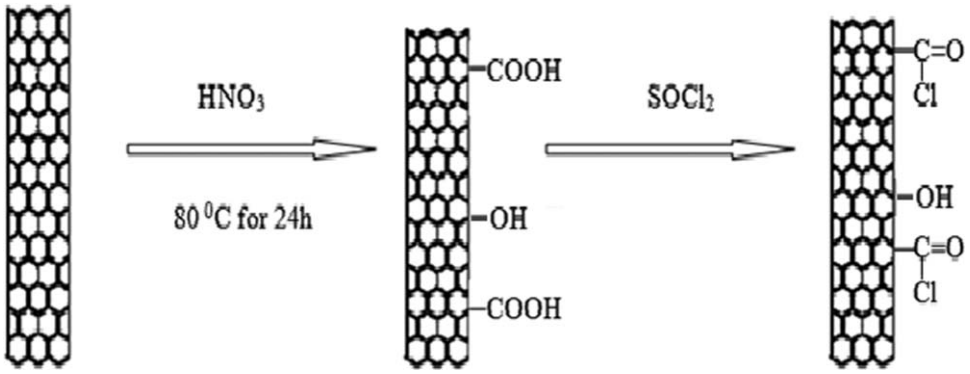

Figure 1. Sketch of the reparation of HNO_3-functionalized MWCNT.[18]

blend viscosity. Indeed, CNT which possess high strength and good thermal and electrical conductivities are considered as a new generation of materials with potential applications in many fields.[11] However, during their dispersion inside polymeric matrices, CNT often form agglomerates due their intrinsic strong Van der Waals attraction forces, their small size and their large specific surface area. Consequently, the dispersion of CNT in a polymeric matrix is still an issue.[12] Various techniques of CNT surface modification, such as covalent or noncovalent functionalization, have been investigated to improve their dispersion in polymers.[13–15] Lee *et al.* have reported the positive effect of the functionalization of multiwall carbon nanotubes (MWCNT) on the electrical conductivity of a MWCNT/polypropylene nanocomposite.[16] Such functionalization was performed through a mixture of H_2SO_4 and HNO_3.

In this study, we optimized a co-continuous (PET/PVDF)/(CB/GR) composite in which we added a small quantity of unfunctionalized and HNO_3- functionalized MWCNT to study their effect on BPPs through-plane electrical resistivity and their impact and flexural yield strengths. It will be demonstrated that the modified MWCNT led to the lowest resistivity (i.e., highest conductivity) due to their better dispersion inside the polymeric PET/PVDF matrix caused by a highest interface interaction.

EXPERIMENTAL

Materials Used

In this work, PET/PVDF system was used as the polymeric phase. PET (commercial grade 9921 W, density of 1.25 g/cm^3, and melt flow index, MFI, of 21.5 g/10 min) was purchased from Eastman. PVDF (commercial grade kynar® 720, density of 1.78 g/cm^3, and MFI of 7.0 g/10 min) was purchased from Arkema. To ensure a high conductivity, high specific area CB (Printex XE-2 from Degussa-Hüls, Germany), synthetic GR (Timrex KS-75 from Timcal America), and MWCNT (Graphitstrength C100 from Arkema) were selected. The GR flakes have an average diameter of 56 μm and MWCNT have an average length of 5μm and an aspect ratio (i.e., length/diameter) of around 400. To limit the thermal degradation of the blends, Irganox® B 215 purchased from Ciba specialty chemicals Canada Inc., was systemically used.

Functionalization of MWCNT

8 g of raw MWCNT were immersed for 1h in 400 mL of concentrated HNO_3, then washed several times with distilled water until the washing water showed no acidity (i.e., neutral pH),[17] and finally dried in oven for 24 h at 80 °C. Covalent functionalization through the oxidation of MWCNT in HNO_3 (a strong acid) causes the opening of the nanotube caps, leading to the formation of carboxylic (-COOH) or hydroxyl (-OH) groups at the surface defect sites. To improve the compatibility between the MWCNT and the polymeric PET/PVDF phase, the above functionalized MWCNT were immersed in 400 mL of thionyl chloride ($SOCl_2$) for 24 h. In fact, after reacting with $SOCl_2$, the carboxylic groups are converted to highly reactive acyl chloride that helps the dispersion of the MWCNT in the (PET/PVDF) polymer phase (Figure 1).

Development of the Conductive Nanocomposites

The conductive (PET/PVDF)/CB and (PET/PVDF)/(CB/GR) composites were prepared using a laboratory twin-crew extruder (Thermohaake polylab system Rheomex CTW 100P). The temperature profile was (270/275/270 °C), from the feeding to the pumping zone, and 270 °C inside the die and the screw rotational speed was fixed constant at 50 RPM.

Some of the above conductive blends were also modified using a small amount of MWCNT. To do this, a Haake Büchler Rheomix internal mixer, with a 40 cm^3 mixing chamber, was used. The mixing temperature and the rotational speed were respectively set at 270 °C and 60 RPM and the whole mixing time was about 10 minutes. The conductive blends were first loaded in the mixing chamber, together with 1% of Irganox® B 215 to avoid thermal degradation, and then the MWCNT were added 5 minutes later.

For further characterization, a series of samples were compression molded (using an automatic 15 tons Carver press) for 5 min at 270 °C under a load of 2 tons, and then cooled down to room temperature using a water cooling system.

SEM, TGA, and Raman Spectroscopy Characterizations

To characterize the morphology of the various conductive nanocomposites and to identify the effect of the MWCNT (both unfunctionalized and HNO_3-functionalized MWCNT) on this morphology, a JEOL scanning electron microscope (SEM; model

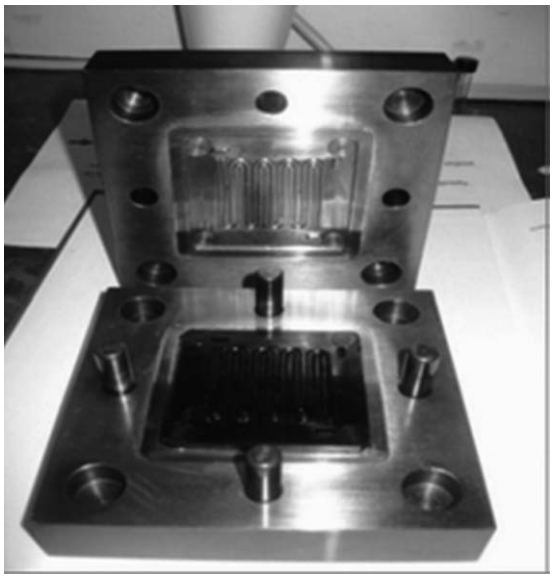

Figure 2. The compression mold showing the gas flow channels and a BP sample.[20]

JSM-840A) was used at a voltage of 15 KV. Thermal stability of the untreated and HNO_3-functionalized MWCNT was investigated in nitrogen atmosphere with a thermogravimetric analyser TGA Q5000 IR (TA Instruments) under a heating rate of 10 °C/min, from 50 to 700 °C. Their corresponding Raman spectra were recorded using a LABRAM 800HR Raman spectrometer (Horiba Jobin Yvon, Villeneuve d'Ascq, France) coupled to an Olympus BX-30 fixed stage microscope, then analysed using Gram/AI 8.0.

Through-Plane Resistivity Characterization

Prepared samples, in the form of discs (25 mm in diameter and 2 mm in thickness) were placed between two highly conductive cylindrical gold-plated electrodes then a compression force of 450 N and a current intensity of 5A were imposed to the electrodes. A highly conductive carbon cloth was placed between each side of tested sample and the electrode to minimize the contact resistance. More details on the experimental technique are presented in a previous work.[19] The volume resistivity ρ (Ω cm) is calculated using the following equation:

$$\rho = \frac{R\pi D^2}{4h} \quad (1)$$

where D (cm) is the electrode diameter, h (cm) is the sample thickness, and R (Ω) is the sample electrical resistance (after subtracting carbon cloth resistance).

Mechanical Characterization

Flexural tests were carried out with respect to ASTM D790 specifications. An Instron test machine (model 5565 with a 50 N load cell) was used under a crosshead speed of 2 mm/min. The three-point support span has an equal length and width of 12 mm × 12 mm. All tests were performed at room temperature and the results correspond to the average of five measurements. The flexural yield strength, σ (MPa), which is a measure of the ability of the material to sustain a loading force F_{max} (N) before sample failure, and the flexural modulus E (GPa) which measures its ability to resist deformation under load, are calculated using the tow following equations:

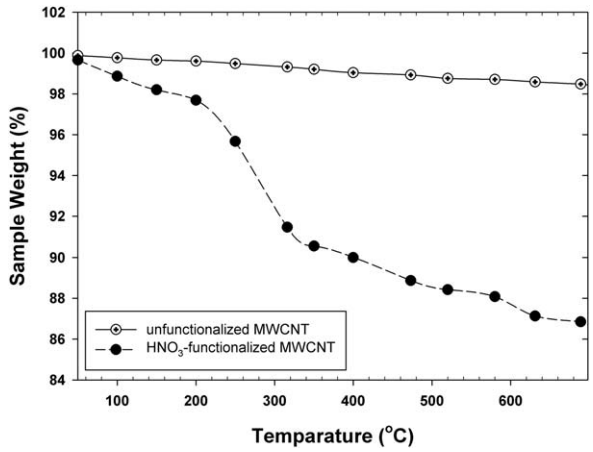

Figure 3. TGA curves of untreated and HNO_3-functionalized MWCNT.

$$\sigma = \frac{3F_{max}L}{2bh^2} \quad (2)$$

$$E = \frac{L^3 m}{4bh^3} \quad (3)$$

where L (mm) is the length of the support span, m is the slope of the tangent at the origin of the load displacement curve, and b (mm) and h (mm) are respectively the width and the thickness of the sample.

Unnotched Charpy impact characterization was performed at room temperature (according to ASTM D256 specifications) using a Tinius Olsen impact machine, model 104 (United states) operating with a Charpy pendulum apparatus (1J). The samples were 12 mm × 100 mm compression-molded with a thickness of 2 mm. Impact characterization data for each characterized sample was averaged from five measurements.

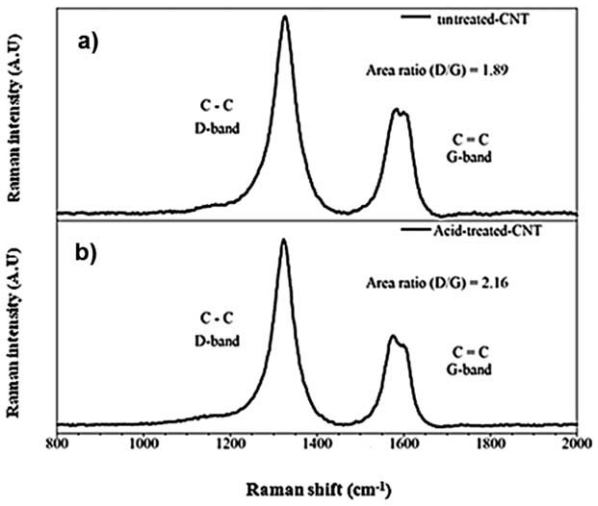

Figure 4. The Raman Spectra of: (a) unfunctionalized, and (b) HNO_3-functionalized MWCNT.

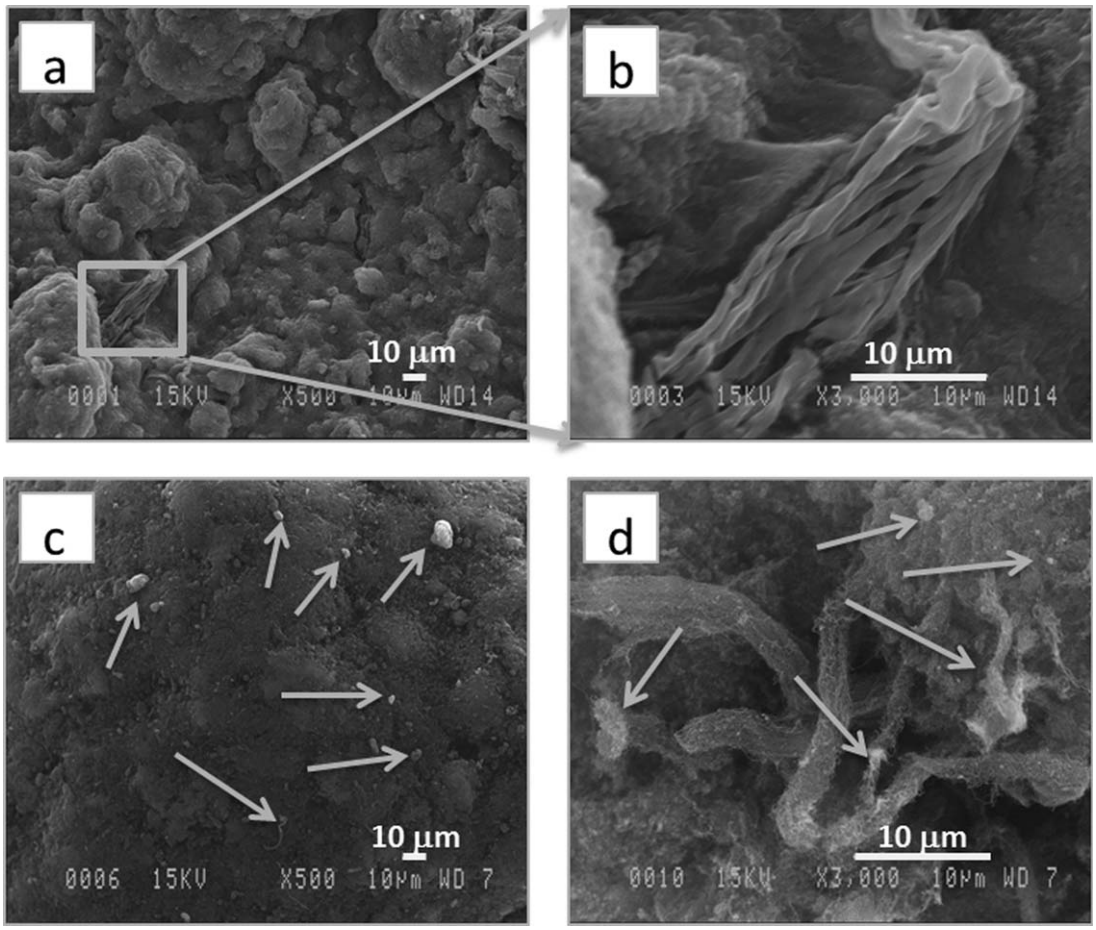

Figure 5. SEM images at two magnification levels of unfunctionalized MWCNT (a,b) and HNO_3-functionalized MWCNT (c,d).

Bipolar Plate Prototype Manufacturing

For further characterization, a series of BPP were compression molded (using an automatic 15 tons Carver press, Auto Series). Selected composites were placed into a specific BP mold with serpentine flow channels and 2 mm in cavity thickness. Figure 2 shows a picture of the mold in its open position, together with a compression molded BPP sample. BP compression molding was done at 280 °C for 15 min under a force of 2 tons. The mold was then cooled down to 190 °C and maintained at this temperature for 30 min to allow the PET phase to crystallize separately without any interference of PVDF phase, which still in its molten state ($T_{m,PVDF}$= 170 °C) and consequently to ensure higher through-plane conductivity, as already explained in our previous work.[20] After PET crystallization, the mold was cooled down to room temperature under cold water, and during this step, both PET and PVDF phases continued to crystallize.

RESULTS AND DISCUSSION

TGA, Raman Spectroscopy, and SEM Characterizations of MWCNT

Figure 3 shows the TGA results corresponding to the weight variation of unfunctionalized and HNO_3-functionalized MWCNT as a function of temperature. It is well known that the organic part of the functionalized MWCNT is removed in the temperature range varying from 250 to 500 °C.[21,22] The content of HNO_3 functionalities can be estimated by calculating the difference between the weight-loss of untreated and HNO_3-functionalized MWCNT. Figure 3 shows that, at 500 °C, the difference between the lost organic weight fraction of HNO_3-functionalized and untreated MWCNT was 10.1% is mainly due to the decomposition of surface-grafted carboxyl (COOH) and hydroxyl (OH) groups after oxidation with HNO_3.

Raman Spectroscopy is a valuable tool for the characterization of MWCNT structure. By comparing the spectra of unfunctionalized and HNO_3-functionalized MWCNT, we can identify their structural destruction due to HNO_3 treatment. Figure 4(a,b) show the two Raman spectra peaks: the so called D-band (assigned to the C—C bond, centred at 1324 cm^{-1}) and the so called G-band (assigned to the C=C bond, centred at 1580 cm^{-1}) for both untreated and HNO_3-functionalized MWCNT, respectively. The area ratio (D/G) for the untreated MWCNT was 1.89. This ratio increased to 2.16 after the treatment MWCNT with HNO_3. This means that HNO_3 treatement led to the breakup of some C=C into C—C, leaving holes 'defects' onto the structure of MWCNT surface.

Figure 5(a–d) show typical SEM images of unfunctionalized and HNO_3-functionalized MWCNT samples. As expected, both samples display tube morphology. Figure 5(a) shows that the

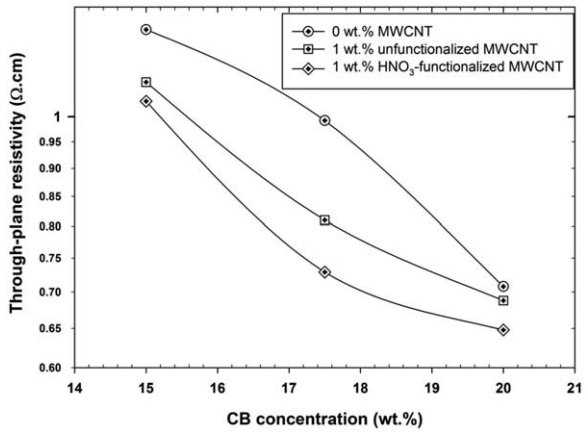

Figure 6. Through-plane resistivity of (PET/PVDF 50:50)/CB-based blends as a function of CB weight concentration: effect of unfunctionalized and HNO_3-functionalized MWCNT.

unfunctionalized MWCNT often form bundles or ropes, as clearly shown by SEM higher magnification shown in Figure 5(b). Conversely, HNO_3-functionalized MWCNT exhibit defects, clearly evident on the high magnification SEM image of Figure 5(d) that shows shorter bundles compared to unfunctionalized MWCNT. This proves that HNO_3 generates functional carboxylic groups sited on the surface of the MWCNT.

Through-Plane Electrical Resistivity and Mechanical Behavior Characterization

Effect of Added CB and MWCNT on the Resistivity of BPP Composites. Figure 6 shows the through-plane electrical resistivity of different (PET/PVDF 50:50)/CB composites as a function of CB weight concentration (curve a). The effect of adding a small quantity (1 wt %) of unfunctionalized and HNO_3-functionalized MWCNT is also shown on the same figure (curves b and c). Curve a shows that the through-plane resistivity decreases from around 1.20 to around 0.71 Ω cm with increasing CB content from 15 to 20 wt %, which is in agreement with previous results already obtained in our research group.[7] Conversely, the addition of a small quantity (1wt %) of MWCNT led to a further decrease in the through-plane resistivity, especially for HNO_3-functionalized MWCNT. For 20 wt % CB, the through-plane resistivity decreased from 0.71 to 0.68 and 0.64 Ω cm with the addition of 1 wt % of unfunctionalized and HNO_3-functionalized MWCNT, respectively. This improvement is due to the fact that MWCNT acts as conductive bridges between the CB particles due to their high aspect ratio of around 400. Their surface modification by HNO_3 improves their compatibility with PET/PVDF polymer phase leading to their higher dispersion, that is, more conductive connections between CB particles.

Synergistic Effect of MWCNT and GR on the Through-Plane Resistivity of (PET/PVDF 50:50)/CB Composites. As mentioned in the introduction section, due to its good lubricating properties, the addition of synthetic GR allowed higher carbon concentrations and consequently helped to improve composite electrical conductivity without any additional processing difficulties. Using the same extruder configuration and the same processing parameters shown above in the experimental section, we were able to incorporate into the (PET/PVDF 50:50)/CB composites up to 20 wt % of additional GR, even at the highest CB concentration of 20 wt %. Figure 7 shows the through-plane electrical resistivity of the different (PET/PVDF 50:50)/CB composites and specifically shows the effect of additional GR (added in different concentrations: 10, 15, and 20 wt %) on composite through-plane resistivity. For each CB concentration, the through-plane resistivity decreases with increasing GR concentration and a significant decrease is also observed with the addition of 1 wt % MWCNT. HNO_3-functionalized MWCNT led to the lowest through-plane resistivity. It is clearly shown that the addition of GR and 1 wt % of MWCNT had a

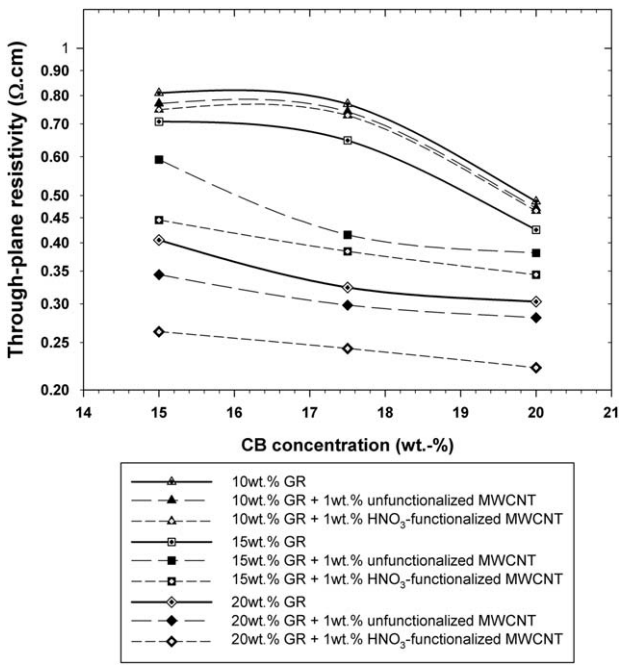

Figure 7. Through-plane electrical resistivity of (PET/PVDF 50:50)/(CB/GR) composites as a function of CB concentration, showing the synergistic effect of GR and unfunctionalized and HNO_3-functionalized MWCNT on composite resistivity.

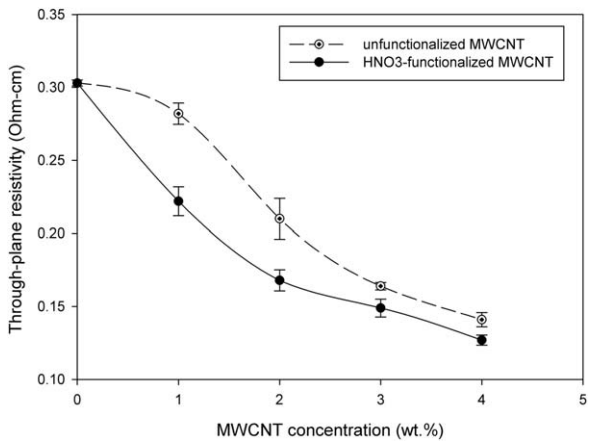

Figure 8. Through-plane resistivity of [60 wt % (PET/PVDF 50:50)]/[40 wt % (CB/GR 50:50)] composites as function of MWCNT weight concentration (wt %).

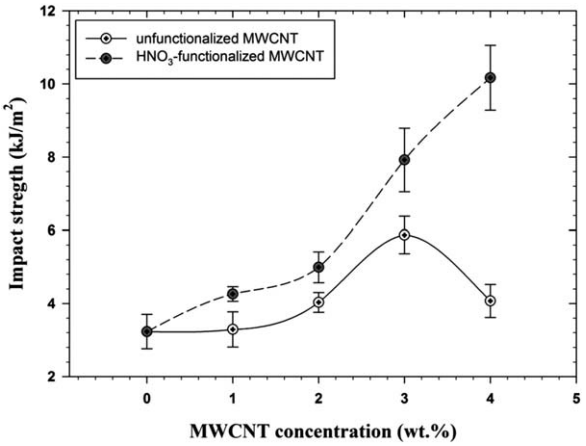

Figure 9. Effect of MWCNT content on the impact strength (Unnotched Charpy) of (PET/PVDF 50:50)/(CB/GR 50:50) composite.

beneficial synergistic effect on composite conductivity. For example, the addition of 20 wt % of GR and 1 wt % of HNO_3-functionalized MWCNT to the (PVDF/PET 50:50)/CB composite already containing 20 wt % of CB led to a decrease in composite through-plane resistivity from 0.71 to 0.22 Ω cm, which could not be achieved with CB only by using the Thermo Haake extruder.

Figure 8 illustrates the effect of MWCNT (both unfunctionalized and HNO_3-functionalized) on the through-plane resistivity of the best composite shown in Figure 7, that is, the composite [60 wt % (PET/PVDF 50:50)]/[40 wt % (CB/GR 50:50)]. Now, MWCNT was added at higher concentrations (up to 4 wt %), replacing the same amount of the polymeric PET/PVDF phase. As shown, a continuous decrease in through-plane resistivity is observed with increasing the concentration of both unfunctionalized and HNO_3-functionalized MWCNT. This confirms the beneficial effect of MWCNT in forming conductive channels between CB and GR particles.[23] The same behavior as that already observed with the addition of 1 wt % MWCNT was also observed for higher MWCNT concentrations, HNO_3-functionalized MWCNT lead to lower through-plane resistivity for concentrations up to 4 wt %.

Mechanical Characterization. In this section, we chose to characterize the Unnotched Charpy impact and flexural properties of the composite [60 wt % (PET/PVDF 50:50)]/[40 wt % (CB/GR 50:50)] that led to the lowest electrical through-plane resistivity and which is used to fabricate the BPP prototype. To improve its mechanical properties, different amounts of MWCNT (varying from 1.0 to 4.0 wt %) were added. Figure 9 shows the impact strength (KJ/m^2) (Unnotched Charpy) of the selected blend, as a function of MWCNT concentration for both unfunctionalized and HNO_3-functionalized MWCNT.

For unfunctionalized MWCNT, the impact strength increased with increasing MWCNT concentration up to 3 wt %. Above this content, the impact strength decreased, as already observed in literature.[24] However, for HNO_3-functionalized MWCNT, the composites showed higher impact strength values with a continuous increase with increasing MWCNT concentration. This is due to the improvement of MWCNT interaction with the PET/PVDF polymeric phase that led to a better MWCNT dispersion and consequently a significant improvement in the impact strength of the corresponding composites.

Figure 10(a,b) show the effect of unfunctionalized and HNO_3-functionalized MWCNT composition on the flexural modulus E (GPa) and the flexural yield strength σ (MPa), respectively, for the same composites presented above. As shown, for both unfunctionalized and HNO_3-functionalized MWCNT, the flexural modulus shows a continuous increase with increasing MWCNT composition. However, HNO_3-functionalized MWCNT led to higher values of E due to the better MWCNT dispersion, a result of their better compatibilization with the (PET/PVDF) polymeric phase. As shown in Figure 10(b), the flexural yield strength shows the same trends as the flexural modulus and HNO_3 treatment of the MWCNT also led to an increase in the flexural yield strength.

Bipolar Plate Prototype Development by Compression Molding

The final step in this work was to manufacture (using the compression molding process and the protocol presented in the experimental section) a bipolar plate prototype from the

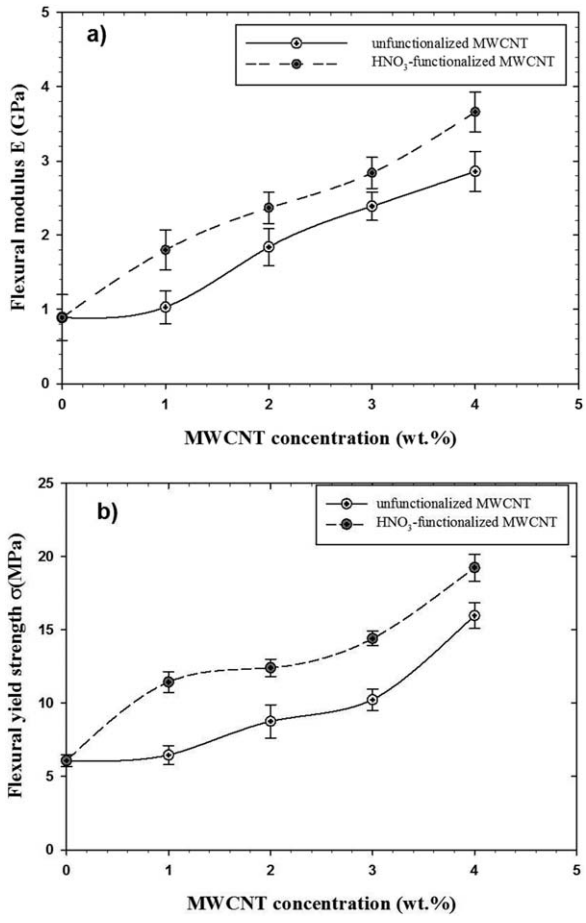

Figure 10. Effect of MWCNT weight concentration on: (a) Flexural modulus E (GPa), and (b) the flexural yield strength σ (MPa) for (PET/PVDF 50:50)/(CB/GR 50:50) composites.

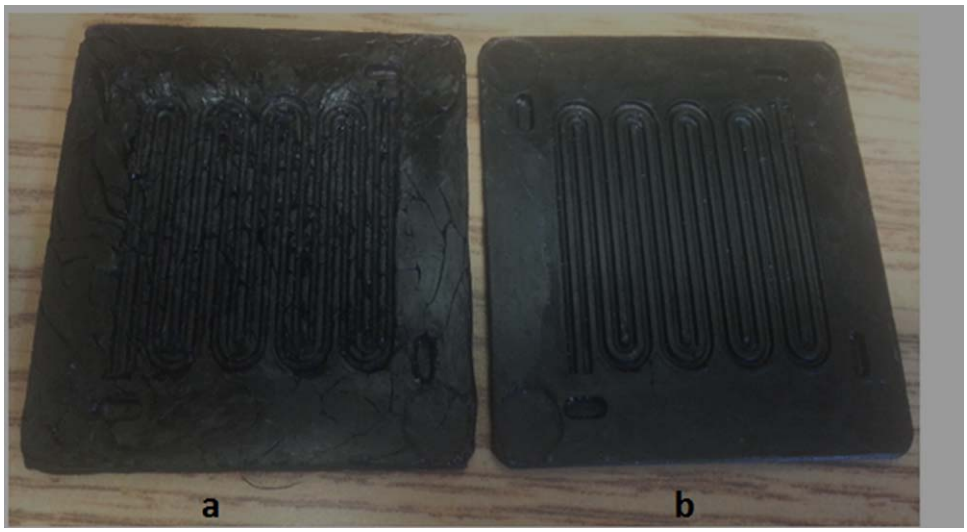

Figure 11. Images of BPP prototypes made from [60 wt % (PET/PVDF 50:50)]/[40 wt % (CB/GR 50:50)]-based blends containing 4 wt % of unfunctionalized MWCNT (picture a) and HNO_3-functionalized MWCNT (picture b). [Color figure can be viewed in the online issue, which is available at wileyonlinelibrary.com.]

composite [60 wt % (PET/PVDF 50:50)]/[40 wt % (CB/GR 50:50)] into which 4 wt % of unfunctionalized or HNO_3-functionalized MWCNT were added. As presented above, these two composites had the lowest through-plane resistivity (i.e., highest electrical conductivity) and the best flexural and impact strengths. Figure 11 shows two BPP prototypes: the first one (picture a), which was developed using unfunctionalized MWCNT, shows a surface with many sink marks (picture a); the second one (picture b) obtained with HNO_3-functionalized MWCNT shows a better surface finish. This is another advantage of the surface treatment of the MWCNT that improves their interfacial adhesion with the polymeric phase, especially the PVDF phase where the carbon additives are largely localized, as already observed.[7,20] The latter BPP prototype was characterized for its through-plane resistivity; the measurements were done directly on BPP periphery, where there are no gas flow channels. The objective was to see the effect of PET crystallization during BPP compression molding on the resistivity. Although the partial orientation of carbon additives parallel to BPP surface (especially GR which is in the form of flat sheets) caused by the compression forces, PET isothermal crystallization at 190 °C helped to maintain a low BPP through-plane resistivity of around 0.12 Ω cm. Compared to our previous results for identical composites composition in terms of CB and GR additives,[7] we decreased BBP through-plane resistivity by 250%, which is considered as a significant improvement.

CONCLUSIONS

In this work, we showed how co-continuous (PET/PVDF)/(CB/GR) conductive composites were prepared and how their electrical through-plane conductivity and impact and flexural strengths were improved by adding small amounts of unfunctionalized and HNO_3-functionalized MWCNT.

After their surface functionalization with HNO_3, MWCNT were characterized by Raman, TGA, and SEM. Their characterization confirmed the formation of functional carboxyl and hydroxyl groups sited on their surface. These new functional groups helped to improve MWCNT dispersion inside the PET/PVDF polymeric phase, preferentially inside the PET phase, as already observed earlier in our previous work,[7] leading to improved mechanical properties and lower through-plane resistivity by forming conductive channels between CB and GR particles. The lowest through-plane resistivity of 0.12 Ω cm was obtained for a [60 wt % (PET/PVDF 50:50)]/[40 wt % (CB/GR 50:50)] composite in which 4 wt % of HNO_3-functionalized MWCNT were added, replacing the same amount of the polymeric PET/PVDF phase. BPP samples developed from this blend showed perfect surface compared to those obtained from same composite but with unfunctionalized MWCNT that showed imperfect surface with many sink marks. Compared to our previous published results, we significantly improved BBP electrical conductivity by decresing it through-plane resistivity by 250%. In the near future, further BPP performance characterization inside a PEMFC stack will be realized under realistic conditions to evaluate the improvements discussed in this work.

ACKNOWLEDGMENTS

The authors are grateful to the Natural Sciences and Engineering Research Council of Canada (NSERC), as well as the Research Center for High Performance Polymer and Composite Systems (CREPEC) for their financial support of this work.

REFERENCES

1. Besmann, T. M.; Klett, J. W.; Henry, J. J., Jr.; Lara-Curzio, E. *J. Electrochem.* **2000**, *147*, 4083.
2. Tawfik, H.; Hung, Y.; Mahajan, D. *J. Power Sources* **2007**, *163*, 755.
3. Hodgson, D. R.; May, B.; Adcock, P. L.; Davies, D. P. *J. Power Sources* **2001**, *96*, 233.

4. Hermann, A.; Chaudhuri, T.; Spagno, P. *J. Hydrogen Energy* **2005**, *30*, 1297.
5. Busick, D.; Wilson, M. U.S. Patent 6,248-467 (**2001**).
6. Yen, C. Y.; Liao, S. H.; Lin, Y. F.; Hung, C. H.; Lin, Y. Y.; Ma, C. C. M. *J. Power Sources* **2006**, *162*, 309.
7. Nguyen, L.; Mighri, F.; Deyrail, Y.; Elkoun, S. *J. Fuel Cells* **2010**, *10*, 938.
8. Bouatia, S.; Mighri, F.; Bousmina, M. *J. Fuel Cells* **2008**, *8*, 120.
9. Fuel Cell Technologies Program Multi-Year Research, Development and Demonstration Plan; U.S. Department of Energy, Fuel Cell Technologies Program: Washington, DC, **2007**.
10. Mighri, F.; Huneault, M. A.; Champagne, M. F. *J. Polym. Eng. Sci.* **2004**, *44*, 755.
11. Zhu, B. K.; Xie, S. H.; Xu, Z. K.; Xu, Y. Y. *J. Compos. Sci. Technol.* **2006**, *66*, 548.
12. Zhang, Z.; Zhang, J.; Chen, P.; Zhang, B.; He, J.; Hu, G. H. *J. Carbon* **2006**, *44*, 692.
13. Tjong, S. C. *J. Mater. Sci. Eng.* **2006**, *53*, 73.
14. Sun, Y. P.; Fu, K.; Lin, Y.; Huang, W. *J. Acc. Chem. Res.* **2002**, *35*, 1096.
15. Tasis, D.; Tagmatarchis, N.; Bianco, A.; Prato, M. *J. Chem. Rev.* **2006**, *106*, 1105.
16. Lee, S. H.; Cho, E.; Jeon, S. H.; Youn, J. R. *J. Carbon* **2007**, *45*, 2810.
17. Jiang, G. H.; Wang, L.; Chen, C.; Dong, X. C.; Chen, T.; Yu, H. J. *J. Mater. Lett.* **2005**, *59*, 2085.
18. Tessonier, J. P.; Villa, A.; Majoulet, O.; Su, D. S.; Schlogl, R. *Angew. Chem. Int. Ed.* **2009**, *48*, 6543.
19. Deyrail, Y.; Mighri, F.; Bousmina, M.; Kaliaguine, S. *Fuel Cells* **2007**, *7*, 447.
20. Song, J.; Mighri, F.; Ajji, A.; Luc, C. *J. Polym. Eng. Sci.* **2012**, *52*, 2552.
21. Christopher, A. D.; James, M. T. *J. Nano Lett.* **2003**, *3*, 1215.
22. Chen, S.; Shen, W.; Wu, G.; Chen, D.; Jiang, M. *J. Chem. Phys. Lett.* **2005**, *402*, 312.
23. Liang, G. D.; Tjong, S. C. *J. Adv. Eng. Mater.* **2007**, *9*, 1014.
24. Zhang, H.; Zhang, Z. *J. Eur. Polym.* **2007**, *43*, 3197.